Journal of Nanobiotechnology

RESEARCH

Open Access

hnRNPA2B1 facilitates ovarian carcinoma metastasis by sorting cargoes into small extracellular vesicles driving myofibroblasts activation

Qiulei Wu[1†], Pan Liu[1†], Xiaoli Liu[1], Guoqing Li[1], Lin Huang[1], Feiquan Ying[1], Lanqing Gong[1], Wenhan Li[1], Jingni Zhang[1], Rui Gao[1], Xiaoqing Yi[1], Linjuan Xu[1], Lili Yu[1*], Zehua Wang[1*] and Jing Cai[1*]

Abstract

Background Ovarian carcinoma (OvCa) metastasis is initiated and boosted by tumor-stroma interactions mediated by small extracellular vesicles (sEVs) containing microRNAs (miRNAs). However, the mechanisms of sorting relevant miRNAs into tumoral sEVs remain elusive.

Results In this study, among the RNA-binding proteins, hnRNPA2B1 was identified as the most significant factor associated with survival in OvCa patients, and its expression was higher in omental metastases compared to paired ovarian lesions. Based on the CRISPR-Cas9 technique, orthotopic xenograft mice revealed a remarkable metastasis-inhibiting effect of hnRNPA2B1-knockdown, accompanied by diminished myofibroblast signals in the omentum. Meanwhile, after hnRNPA2B1-knockdown, OvCa-sEVs largely lost the ability to promote omental metastasis and myofibroblast activation in vivo and in vitro. High-throughput miRNA sequencing of sEV cargoes revealed that UAG motif-containing miRNAs were significantly affected by hnRNPA2B1, and RNA immunoprecipitation (RIP) verified their direct binding to hnRNPA2B1. In pull down assays, the miRNAs with mutated UAG motif exhibited decreased binding capacity to hnRNPA2B1. The myofibroblasts activated by OvCa-sEVs could promote tumor metastasis, and this effect was notably impacted by manipulating hnRNPA2B1, related sEV-miRNAs, and PI3K/AKT signaling.

Conclusions These findings highlight the miRNA sorting to sEVs mediated by hnRNPA2B1 as an important mechanism involved in OvCa metastasis, which may illuminate new therapeutic strategies.

†Qiulei Wu and Pan Liu contributed equally to this work.

*Correspondence:
Lili Yu
yulili@hust.edu.cn
Zehua Wang
zehuawang@hust.edu.cn
Jing Cai
jingcai@hust.edu.cn

Full list of author information is available at the end of the article

Graphical Abstract

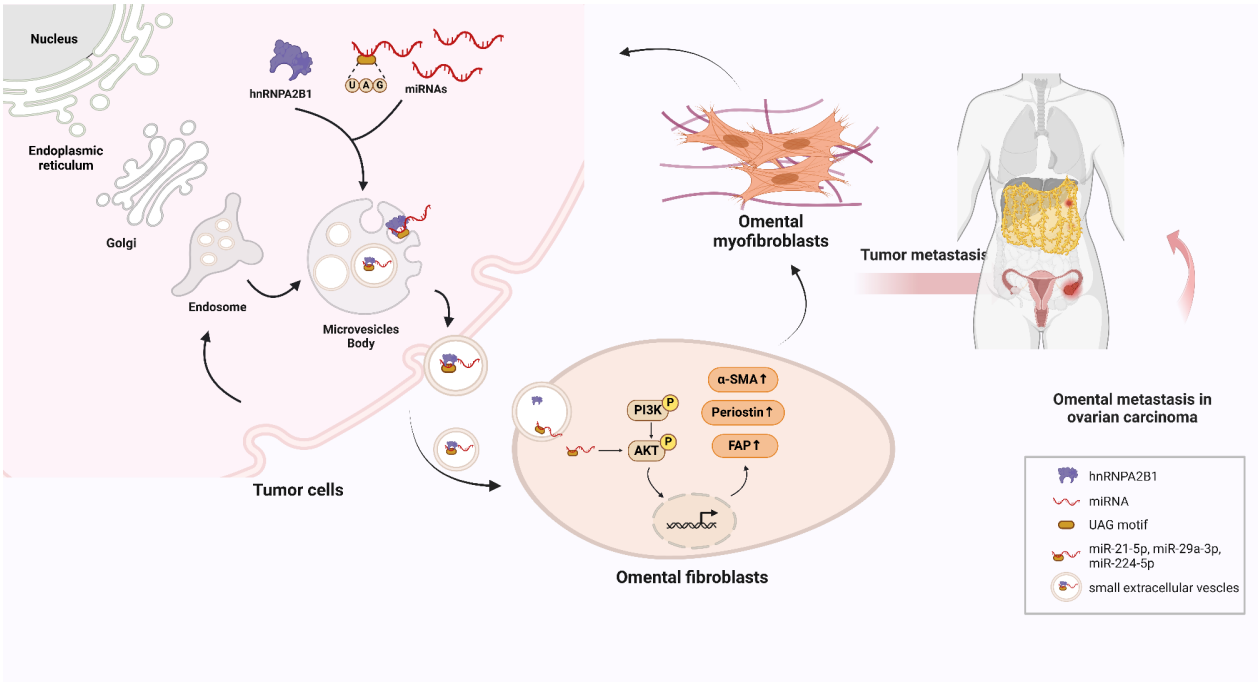

Keywords Ovarian cancer, Cancer-associated fibroblasts, RNA binding protein, Exosome, Noncoding RNA

Background

Ovarian carcinoma (OvCa) is a malignant gynecological tumor with a particularly poor prognosis [1]. Most patients with OvCa are initially diagnosed with peritoneal metastasis, which limits their prognosis. Therefore, it is imperative to investigate the molecular mechanism of tumor metastasis in OvCa.

Small extracellular vesicles (sEVs), nanoscale vesicles that are enclosed by a cell-derived membrane, play an essential role in the tumor microenvironment (TME) [2]. Fibroblasts, prevalent in the tissue matrix, are pivotal for supporting extracellular matrix production and maintaining tissue structure stability. In tumors, fibroblasts undergo phenotypic transformation into cancer-associated fibroblasts (CAFs), acquiring specific molecular alterations that promote extracellular matrix deposition, cytokine secretion, and other tumor-promoting functions [3]. CAFs are the predominant stromal cells in the TME. Unlike a monoclonal population, CAFs consist of a dynamic collection of fibroblast subpopulations with distinct characteristics and functions. Our previous study demonstrated that omental fibroblasts can differentiate into cancer-associated myofibroblasts (myCAFs), a unique category of CAFs [4]. myCAFs, characterized by enhanced extracellular matrix synthesis and stromal contraction promotion, exhibit high expression of the smooth muscle actin gene *ACTA2* [3]. Studies have shown that myCAFs facilitate tumor metastasis by secreting type V collagen [5]. Mounting evidence has indicated that sEV-miRNAs are essential for remodeling the TME and promoting tumor metastasis [6]. However, the mechanism of sEV cargo-loading has not yet been fully elucidated.

Certain miRNAs are preferred for sorting into sEVs [7]. Four potential pathways for miRNA sorting into sEVs have been identified in current studies, including the type 2 neutral sphingomyelinase (nSMase2)-dependent pathway [8], the miRNA sequence 3' end-dependent pathway [9], the miRNA-induced silencing complex-related pathways [10], and the RNA-binding protein (RBP) pathway [11]. Generally, the specific motifs within these miRNAs guide the sorting process. Studies have demonstrated that RBPs are essential for deciding which miRNAs are selected for sEV enrichment [11–14]. RBPs are crucial throughout the RNA life cycle. To date, more than 1 500 RBPs have been recognized in humans. These proteins can be categorized into more than fifteen distinct types according to their diverse functions, including epithelial splicing regulatory proteins, cytoplasmic polyadenylation element binding protein family members, and heterogeneous nuclear ribonucleoprotein family members (hnRNPs) [15, 16]. Several studies have indicated that

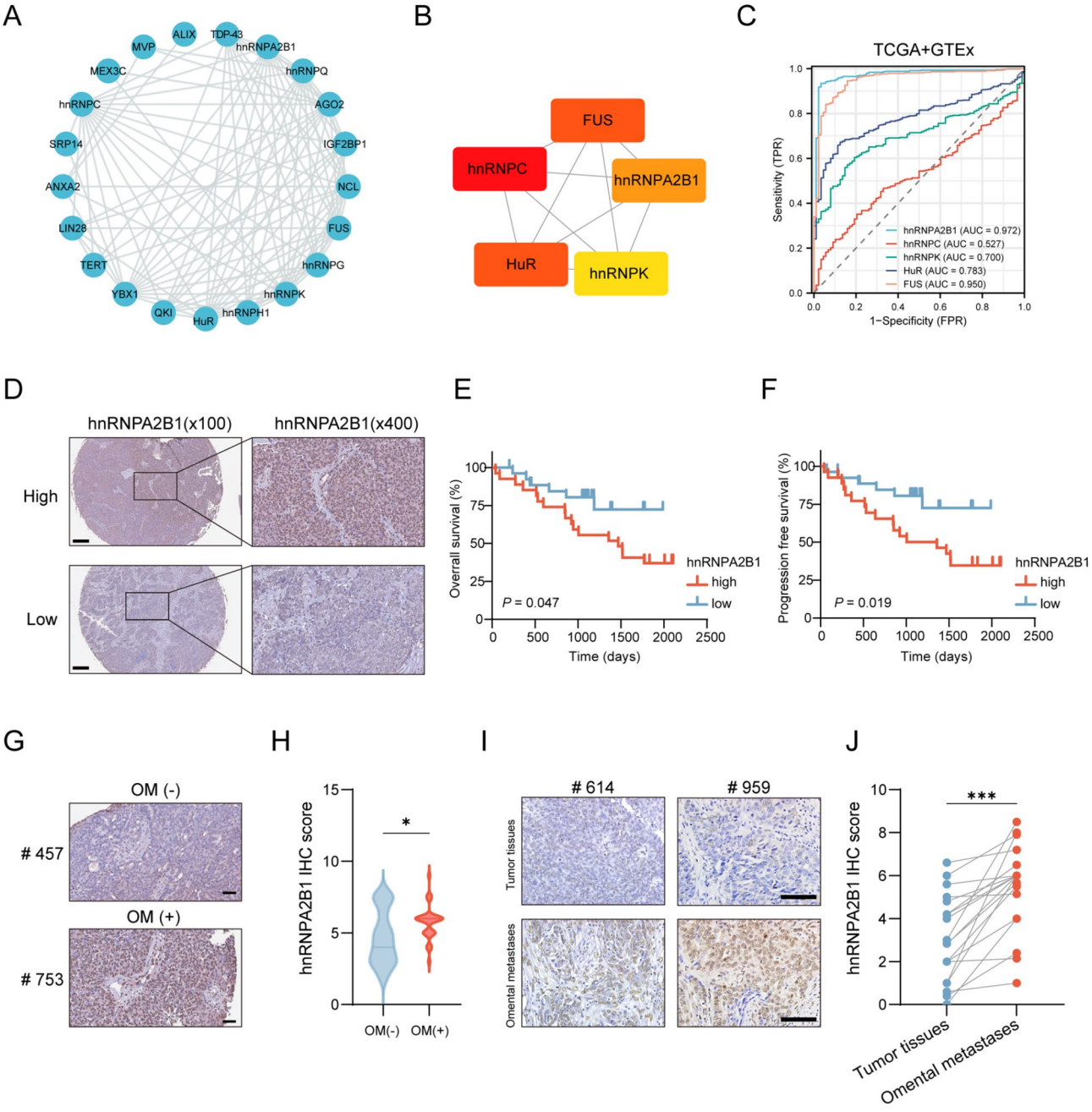

Fig. 1 High hnRNPA2B1 expression is associated with poor prognosis and omental metastasis in OvCa patients. (**A**) The PPI network of RNA-binding proteins involved in the sorting of miRNAs into small extracellular vesicles (sEVs). (**B**) The top five critical molecules identified by the PPI network based on the CytoHubba MCC algorithm by Cytoscape software. (**C**) ROC curves of hnRNPA2B1, hnRNPC, hnRNPK, HuR, and FUS to determine the sensitivity and specificity of the diagnosis of OvCa or normal patients based on the TCGA and GTEx datasets. (**D**) Representative IHC images of hnRNPA2B1 in OvCa tissues. Scale bar, 250 μm. ($n = 54$). (**E-F**) Kaplan – Meier curve of overall survival (**E**) and progression free survival (**F**) in OvCa patients with different hnRNPA2B1 levels ($n = 54$). (**G-H**) Representative IHC images (**G**) and quantification (**H**) of hnRNPA2B1 in OvCa tissues with or without omental metastasis (OM). Scale bar, 50 μm. ($n = 54$). (**I**) Representative IHC images of hnRNPA2B1 in tumor tissues and paired omental metastases. Scale bar, 100 μm. (**J**) Comparison of hnRNPA2B1 levels between the tumor tissues and paired omental metastases ($n = 19$). $^{*}P < 0.05$, $^{***}P < 0.001$

certain members of the RBP family are involved in the process of sEV-miRNA sorting [11]. However, the exact mechanisms by which RBPs regulate sEV-miRNAs in OvCa cells have not been fully elucidated.

In this study, we identified the potential RBPs involved in sEV-miRNA sorting in OvCa through bioinformatics screening combined with clinical correlation analysis, and hnRNPA2B1 was found to be the key RBP involved in promoting tumor progression. hnRNPA2B1, a member

Table 1 Correlation between hnRNPA2B1 and clinicopathological characteristics of OvCa patients

Characteristics	Total	hnRNPA2B1 level		*P*-value
	(*n* = 54)	High (%)	Low (%)	
Age (years)				1
< 50	20	10(50)	10(50)	
≥ 50	34	17(50)	17(50)	
FIGO stage				0.003
Stage I- II	16	3(18.8)	13(81.3)	
Stage III- IV	38	24(63.2)	14(36.8)	
Histological type				0.008
HGSOC	37	23(62.2)	14(37.8)	
Non-HGSOC	17	4(23.5)	13(76.5)	
Omentum metastasis				0.013
No	23	7(30.4)	16(69.6)	
Yes	31	20(64.5)	11(35.5)	
Lymph metastasis				0.026
No	41	17(41.5)	24(58.5)	
Yes	13	10(76.9)	3(23.1)	
Appendix metastasis				
No	43	20(46.5)	23(53.5)	0.311
Yes	11	7(63.6)	4(36.4)	

HGSOC, High grade serous ovarian cancer; FIGO, International Federation of Gynecology and Obstetrics

of the hnRNP family, is essential for various aspects of RNA biology, such as DNA damage repair, alternative splicing, and RNA transport [17]. Here, we revealed the metastasis-promoting role of hnRNPA2B1 in OvCa through tumor tissues analysis of patients and spontaneous orthotopic tumor models in mice. Moreover, high-throughput miRNA sequencing of sEVs derived from tumor cells was employed to screen for sEV-miRNAs regulated by tumoral hnRNPA2B1, and omental-derived primary fibroblasts (ODPFs) were utilized to investigate the functions of these sEVs and miRNAs. Our efforts will reveal the mechanism through which RBPs promote tumor metastasis through sEV-cargo sorting, indicating that patients with high hnRNPA2B1 levels would benefit from individualized treatment.

Materials and methods

Clinical samples

The specimens used in this study were approved by the Ethics Committee of Union Hospital, Tongji Medical College, Huazhong University of Science and Technology, and the patients provided informed consent. All patients were pathologically diagnosed with OvCa after surgery. Paraffin embedding was performed in patients with OvCa. The collected tumor tissues from the fifty-four patients with OvCa were embedded in paraffin to make a tissue chip. A total of nineteen primary tumors and matched omental metastases were used for the immunohistochemistry experiments. ODPFs were extracted from the omental tissues of sixteen OvCa patients. The sEVs derived from ascites were isolated from three OvCa patients.

Immunohistochemistry (IHC) staining

The methods were described in previously reports [18]. The concentrations of the antibodies used are provided in Table S1. The results were evaluated via the following formula: staining intensity (none = 0, weak = 1, medium = 2, strong = 3) multiplied by the staining area (none = 0, less than 30% = 1, between 30% and 60% = 2, greater than 60% = 3). The product of the staining intensity and staining area represents the expression level of the target protein.

Cell lines and cell culture

The OvCa cell lines SK-OV-3, ID8, IGROV-1, Caov-3, ES-2, OVCAR-3, and OVCAR-4 were authenticated via STR analysis and matched with the cell bank. Among them, the pathological type of the OVCAR-3 and OVCAR-4 cell lines was high-grade serous carcinoma. ES-2-HM (ES-2 highly metastatic) cells constitute a highly metastatic subline established by our research group. The experimental procedures were performed as previously described [19]. All the cells were cultured in DMEM/F12 medium (BasalMedia, China) supplemented with 10% fetal bovine serum (ExCell Bio, China) in a 37 °C incubator with 5% CO_2.

Cell transfection

The hnRNPA2B1-knockdown cell line was generated via the CRISPR/Cas9 technique with single guide RNA (sgRNA) by the Jikai Gene Company (Shanghai, China). The miRNA mimics were purchased from RiboBio (Guangzhou, China). HiPerFect (Qiagen, Germany) was used for the transfection assays. The sequences of the sgRNAs and the miRNA mimics used are shown in Table S2.

Omental-derived primary fibroblast extraction

Fresh omental tissues from patients diagnosed with OvCa at our hospital were surgically removed and used to isolate ODPFs. The isolation and extraction of fibroblasts were performed according to previous methods [4]. All ODPFs used in this study were 2nd- to 5th-generation cells. The patients are shown in Table S3.

sEV isolation and characterization

The sEVs derived from tumor cells were isolated from the conditioned medium as described previously [4]. An Optima XPN-100 Ultracentrifuge (Beckman Coulter, USA) was used in this study. The tumor cells were cultured in complete medium containing sEV-depleted fetal bovine serum, after which the supernatant was collected. The conditioned medium was centrifuged at 300 g for 10 min, 2 000 g for 10 min, and 10 000 g for 30 min

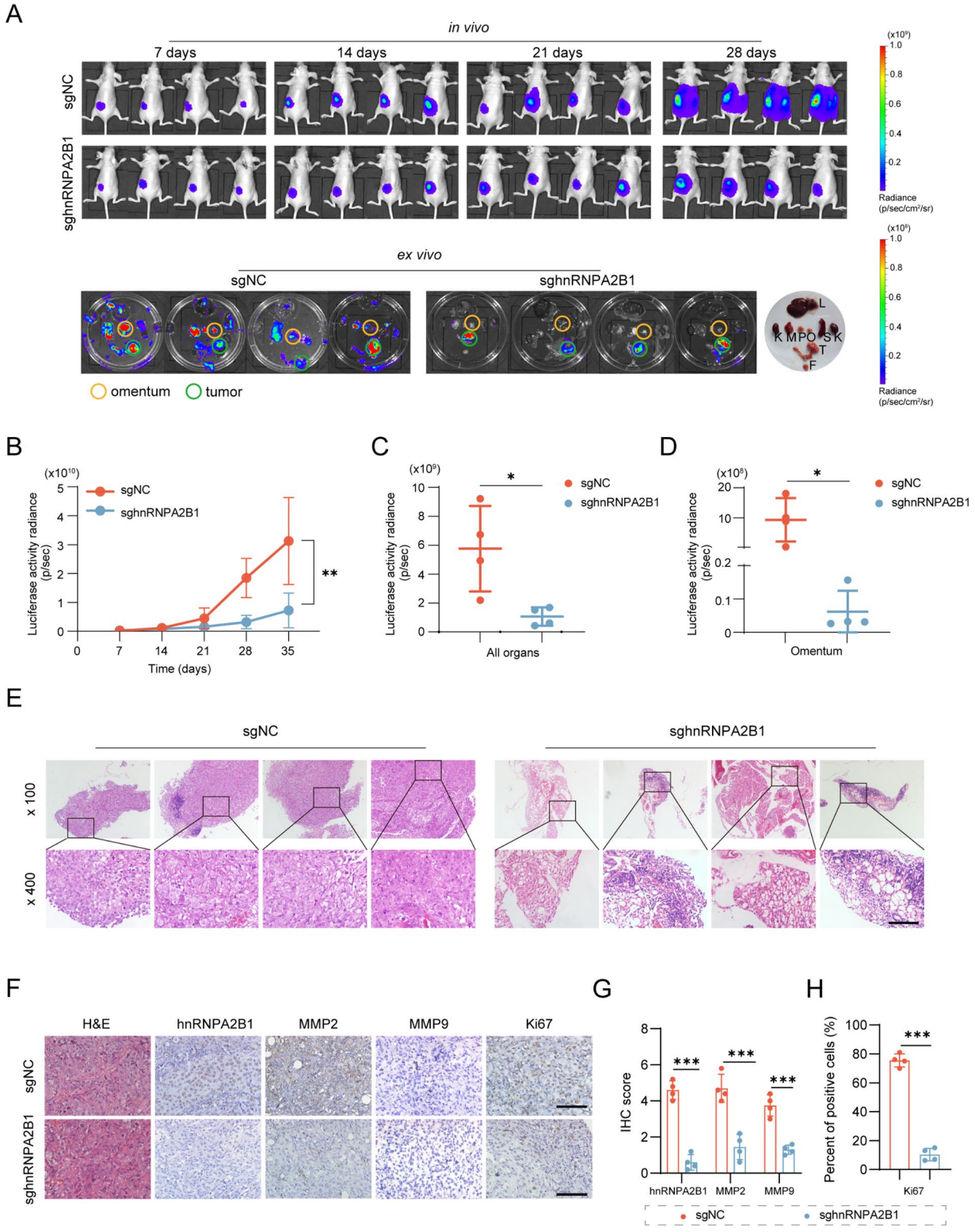

Fig. 2 Knockdown of hnRNPA2B1 suppresses tumor metastasis in vivo. (**A**) Representative bioluminescence images of orthotopic ovarian xenografts generated from luciferase-labeled ES-2-HM cells with ($n=4$) or without ($n=4$) hnRNPA2B1 knockdown in vivo (above), and from abdominal organs isolated ex vivo (below). L for liver, K for kidney, M for mesentery, P for pancreas, O for omentum, S for spleen, T for tumor, and F for fat pad. (**B**) The total fluorescence intensity at different observation points. (**C-D**) Scatter plot showing the bioluminescence signals of all abdominal organs (**C**) and omentum (**D**) ex vivo. (**E**) Representative H&E images of omental tissues from the nude mice described above. Scale bar, 100 μm. (**F-H**) Representative H&E images, IHC (**F**) images and quantification of hnRNPA2B1, MMP2, MMP9 (**G**), and Ki67 (**H**) in tumors of mice. Scale bar, 100 μm. *$P<0.05$, **$P<0.01$, ***$P<0.001$

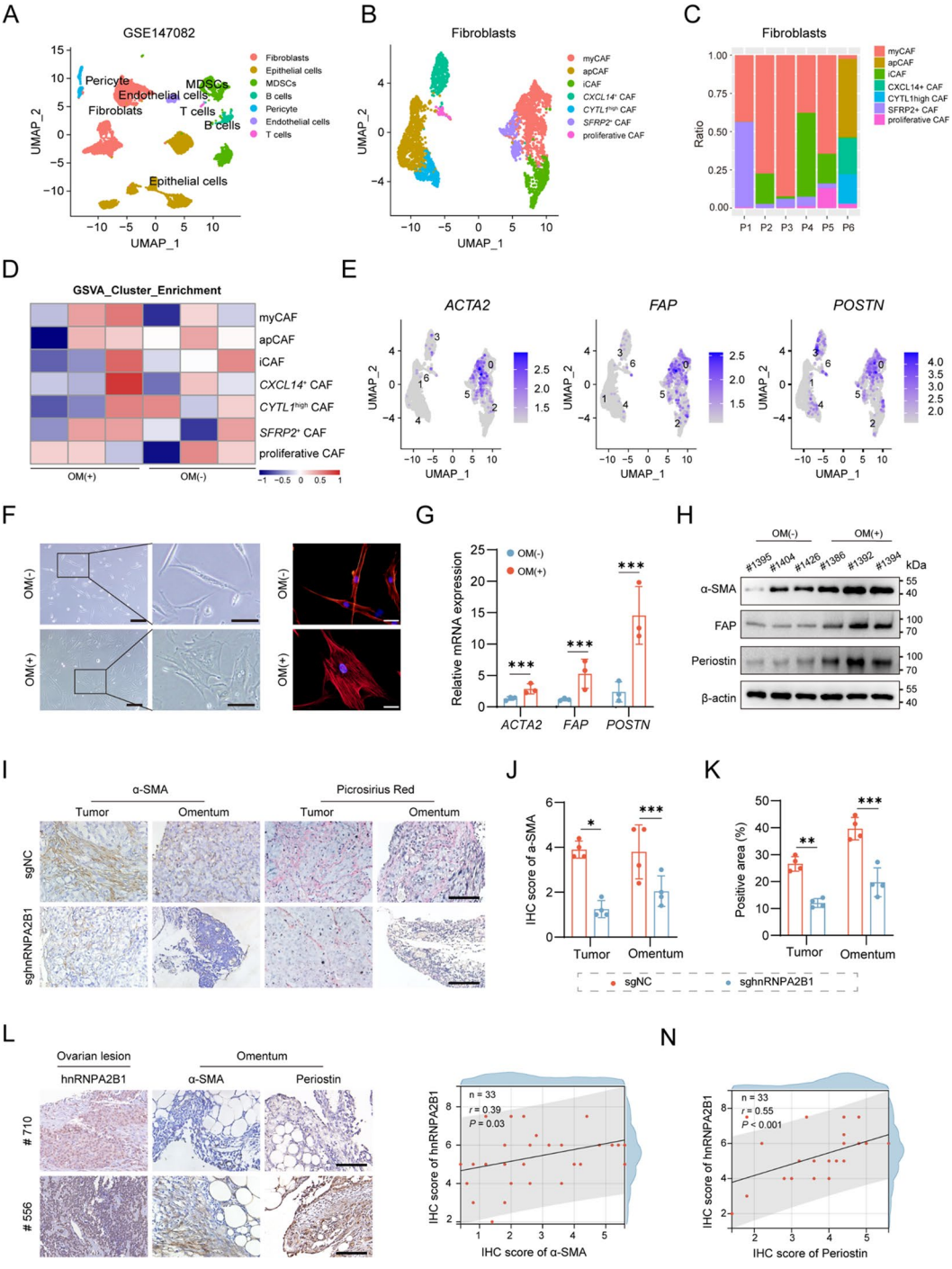

Fig. 3 Tumoral hnRNPA2B1 expression is positively correlated with omental myofibroblasts. (**A**) UMAP plot showing the distinct cell types identified by marker genes from OvCa patients in the GSE147082 dataset. (**B**) UMAP plot of cancer-associated fibroblast (CAFs) showing seven clusters. (**C**) Bar plots showing the proportions of each CAFs cluster in every sample. (**D**) Heatmap displaying GSVA scores for each CAFs cluster (GSE147082) in OvCa patients (GSE193875) with or without omental metastasis (OM). (**E**) UMAP plot showing the expression of *ACTA2*, *FAP*, and *POSTN* in all CAFs clusters. (**F**) Representative morphology of #1357 omental-derived primary fibroblasts (ODPFs) (without omental metastasis) and #1332 ODPFs (with omental metastasis) determined by bright-field microscopy (left) and after F-actin staining (right). Scale bar, 200 μm (left). Scale bar, 100 μm (middle panel). Scale bar, 50 μm (right). (**G**) qRT–PCR analysis of *ACTA2*, *FAP*, and *POSTN* expression in ODPFs. (**H**) Western blot analysis of the α-SMA, FAP, and periostin level in ODPFs. (**I-K**) Representative IHC images and quantification of α-SMA and picrosirius red staining in tumor tissues and omental tissues from orthotopic xenografts generated from ES-2-HM^{sgNC} or ES-2-HM^{sghnRNPA2B1} cells. Scale bar, 100 μm. (**L**) Representative IHC images of hnRNPA2B1 in ovarian lesions, and showing the expression of α-SMA or periostin in corresponding paired omental tissues. Scale bar, 100 μm. (**M-N**) Scatter plot showing the correlation between hnRNPA2B1 levels in ovarian lesions and α-SMA or periostin levels in paired omental tissues. *$P < 0.05$, **$P < 0.01$, ***$P < 0.001$

at 4℃. Then, the supernatant was filtered using a filter membrane of 0.22 μm (Millipore, USA) and centrifuged at 120 000 g at 4℃ for 70 min. The precipitate obtained by centrifugation was resuspended in 100 μL of PBS. For ascites sEV, after obtaining fresh ascites in the operating room, the supernatant was collected after centrifugation at 4℃ at 4 500 g for 20 min. The other extraction steps were the same as those of sEV derived from tumor cells. To determine the location of sEVs miRNA, sEVs were treated with RNase (YEASEN, China) in the presence or absence of 1% Triton X-100 for miRNA detection.

In vivo mouse models

Five-week-old female BALB/c nude mice were purchased from Beijing Vital River Laboratory Animal Technology (Beijing, China). To explore the role of hnRNPA2B1 in OvCa metastasis, a total of eight mice were randomly divided into two groups. Luciferase-labeled ES-2-HM^{sgNC} or ES-2-HM^{sghnRNPA2B1} cells were used to construct spontaneous orthotopic tumor models in nude mice, and dynamic imaging monitoring was performed. To explore the role of sEVs mediated by hnRNPA2B1 in promoting metastasis, spontaneous orthotopic tumors formed from luciferase-labeled ES-2 cells were established. A total of twelve mice were randomly divided into three groups, and then injected intraperitoneally once every three days for two weeks with PBS, 50 μg of sEV^{sgNC}, or sEV^{sghnRNPA2B1}. To validate the metastasis-promoting role of myCAFs activated by tumoral hnRNPA2B1 in vivo. A total of three nude mice were intraperitoneally injected with luciferase-labeled ES-2^{sgNC} cells, while twelve nude mice were intraperitoneally injected with luciferase-labeled ES-2^{sghnRNPA2B1} cells. The twelve mice injected with ES-2^{sghnRNPA2B1} cells were randomly divided into four groups, and treated with DMSO, agomiR-NC, agomiR-21/29/224 or agomiR-21/29/224 combined with MK2206.

RNA extraction and qRT-PCR

The qRT-PCR primers used are listed in Table S4. β-actin served as the internal reference for mRNA, whereas U6 served as the internal reference for miRNA. Each sample was tested in triplicate, with at least three biological replicates conducted for each experiment.

MiRNA pull-down

The RNA pull-down kit (Guangzhou Boxin Biotechnology Co., Ltd., Guangzhou, China) was used according to the manufacturer's protocol. The miRNA probe, which was labeled with biotin, and the mutated miRNA probe were incubated with streptavidin magnetic beads. Then, the mixture was subsequently incubated with OvCa cell lysate. Afterwards, the magnetic beads were washed with lysis buffer, and the hnRNPA2B1 protein bound to these beads was analyzed through Western blotting analysis. The sequences are provided in Table S2. Each experiment was repeated a minimum of three times.

RNA immunoprecipitation (RIP)

A RIP kit (Guangzhou Boxin Biotechnology Co., Ltd., Guangzhou, China) was used to evaluate the interactions between hnRNPA2B1 and miRNAs. Specifically, the OvCa cells were rinsed twice with cold PBS, scraped from the plates and transferred to a centrifuge tube. The Cells were collected by centrifugation, and the supernatant was discarded. The cells were subsequently incubated with an RIP buffer containinghnRNPA2B1 antibody-conjugated magnetic beads. After washing five times, the immunoprecipitated RNAs were purified for analysis. The expression of miRNAs was tested via qRT-PCR. Each experiment was repeated at least three times.

Statistical analysis

The means ± standard deviations were used to represent the experimental data results. Student's t test (normal distribution) and the Mann-Whitney U test (non-normal distribution) were used to compare two groups. One-way ANOVA was used for multi-group comparisons. The Kaplan-Meier method and log-rank method were used for survival analysis. $P < 0.05$ was considered to indicate statistical significance. GraphPad Prism software (version 9.0, USA), SPSS software (version 27, USA), and R-Studio software (version 4.1.2, USA) were used.

Results

High hnRNPA2B1 expression is associated with poor prognosis and omental metastasis in OvCa patients

To investigate the existence of the sEV-miRNA sorting phenomenon in OvCa, the GSE103708 dataset was analyzed. The results revealed significant differences between the miRNAs identified in OvCa cells and those detected in their corresponding sEVs (Fig. S1A-B). Proteins identified as the potential RBPs involved in sEV-miRNA sorting in OvCa include members of the hnRNP family (hnRNPA2B1, hnRNPC, hnRNPG, hnRNPH1, hnRNPK, and hnRNPQ), as well as YBX1, HuR, AGO2, IGF2BP1, MEX3C, ANXA2, ALIX, NCL, FUS, TDP-43, MVP, LIN28, SRP14, QKI, and TERT [11]. Among them, hnRNPA2B1, hnRNPC, hnRNPK, HuR, and FUS were identified as the top 5 key molecules on the basis of the CytoHubba MCC algorithm by Cytoscape software through the PPI network (Fig. 1A-B). Further analysis of the TCGA and GTEx datasets was used to determine the sensitivity and specificity of the diagnosis of OvCa or normal patients, and the results revealed that hnRNPA2B1 had the highest area under the curve among the top 5 key molecules (Fig. 1C), indicating its potential clinical value. Additionally, the expression of *HNRNPA2B1* was higher

in OvCa tissues than in normal tissues in the GSE27651 database (Fig. S1C). High *HNRNPA2B1* expression was significantly associated with advanced International Federation of Gynecology and Obstetrics (FIGO) stage of OvCa patients in the GSE14407 database and poor survival of OvCa patients in the TCGA database (Fig. S1D-E). These results indicate that hnRNPA2B1 may play an important role in OvCa.

IHC experiments were subsequently conducted on tumor tissue chips obtained from fifty-four patients with OvCa to assess the level of hnRNPA2B1. The patient information is shown in Table 1. The results revealed that high hnRNPA2B1 levels were strongly correlated with advanced FIGO stage and omental metastasis (Fig. 1D; Table 1). Kaplan-Meier survival analysis of the fifty-four patients with OvCa revealed that OvCa patients with high hnRNPA2B1 levels had significantly shorter overall survival (OS) and progression-free survival (PFS) than those with low hnRNPA2B1 levels (Fig. 1E-F). As shown in Fig. 1G-H, a higher level of hnRNPA2B1 in tumor tissues was observed in patients with omental metastasis than in patients without metastasis. Furthermore, a total of nineteen primary tumors, along with their matched omental metastases, were utilized in IHC experiments, and the results revealed that the expression of hnRNPA2B1 in tumor tissue was lower than that in paired omental metastases (Fig. 1I-J). These findings suggest that hnRNPA2B1 might be related to the omental metastasis of OvCa.

Knockdown of hnRNPA2B1 suppresses tumor metastasis in vivo

Further studies were conducted to explore the role of hnRNPA2B1 in promoting metastasis in vivo. First, we assessed the level of hnRNPA2B1 in OvCa cell lines, and we found that hnRNPA2B1 expression was upregulated in the ES-2 highly metastatic cells (ES-2-HM cells) compared with that in ES-2 cells (Fig. S2A-C). We then used ES-2-HM and OVCAR-4 cells to knock down hnRNPA2B1 via the CRISPR-Cas9 technique (Fig. S2D-E). Furthermore, luciferase-labeled ES-2-HM^{sgNC} or ES-2-HM^{sghnRNPA2B1} cells were used to construct spontaneous orthotopic tumor models in nude mice, and the bioluminescence signal was dynamically monitored through in vivo imaging (Fig. 2A). The results revealed that the bioluminescence signal density in the sghnRNPA2B1 group decreased rapidly compared with that in the sgNC group (Fig. 2B). The signal change in each mouse's fluorescence signal was shown in Fig. S2F. Ex vivo bioluminescence detection revealed that the bioluminescence intensity of abdominal organs and omental tissues in the sgNC group was greater than that in the sghnRNPA2B1 group (Fig. 2C-D). H&E staining of omental tissues revealed omental metastasis in the sgNC group, whereas inflammatory infiltration was observed in the sghnRNPA2B1 group (Fig. 2E). Using GEPIA2 (TCGA datasets), our study identified significant positive correlations between hnRNPA2B1 and the gelatinases MMP2 and MMP9 in OvCa (Fig. S2G). The levels of MMP2, MMP9, Ki67, and hnRNPA2B1 in tumor tissues from nude mice were significantly lower in the sghnRNPA2B1 group than in the sgNC group (Fig. 2F-H). In conclusion, these findings indicate that hnRNPA2B1 could increase the colonization ability of tumor in omental metastases.

Tumoral hnRNPA2B1 is positively correlated with omental myofibroblasts

To assess which of the most essential cells in the TME promote OvCa omental metastasis, the GSE147082 dataset was used to evaluate the distribution of the subpopulations of omental tissues from OvCa patients at the single-cell level. The results revealed that fibroblasts composed the majority of the subpopulations (Fig. 3A, Fig. S3A-D). Among these fibroblast clusters, myCAFs constituted the greatest proportion of cells (Fig. 3B-C). Gene set variation analysis (GSVA) analysis of GSE193875 and GSE147082 indicated that the myCAFs was more common in omental metastases than in non-omental metastases (Fig. 3D). The marker genes associated with myCAFs were identified as *ACTA2*, *FAP*, and *POSTN* (Fig. 3E, Fig. S3E-H). These results indicate that myCAFs may play an important role in the OvCa omental metastasis.

We subsequently extracted the ODPFs from the omental tissues of OvCa patients. Under light microscopy and immunofluorescence staining, compared with ODPFs without metastasis, ODPFs derived from metastatic omental tissues presented enlarged cell bodies and elongated cytoskeletal structures (Fig. 3F). The myCAFs markers α-SMA, FAP, and periostin, were more abundant in ODPFs isolated from omental metastases than in ODPFs isolated from non-omental metastases, as revealed by qRT-PCR and Western blotting assays (Fig. 3G-H, Fig. S4A). Furthermore, tumor tissues and omental tissues were isolated from spontaneous orthotopic tumor models mice via ES-2-HM^{sgNC} or ES-2-HM^{sgHNRNPA2B1} cells. Then, picrosirius red staining was used to detect collagen deposition in the stroma, and α-SMA staining was used to detect myCAF activation. The results revealed a significant reduction in the level of α-SMA and in the area of picrosirius red staining in tumor tissues and omental tissues from the sghnRNPA2B1 group compared with those from the sgNC group, suggesting that hnRNPA2B1 promotes collagen deposition and myofibroblast activation (Fig. 3I-K). Furthermore, tumoral hnRNPA2B1 expression was positively correlated with the levels of α-SMA and periostin

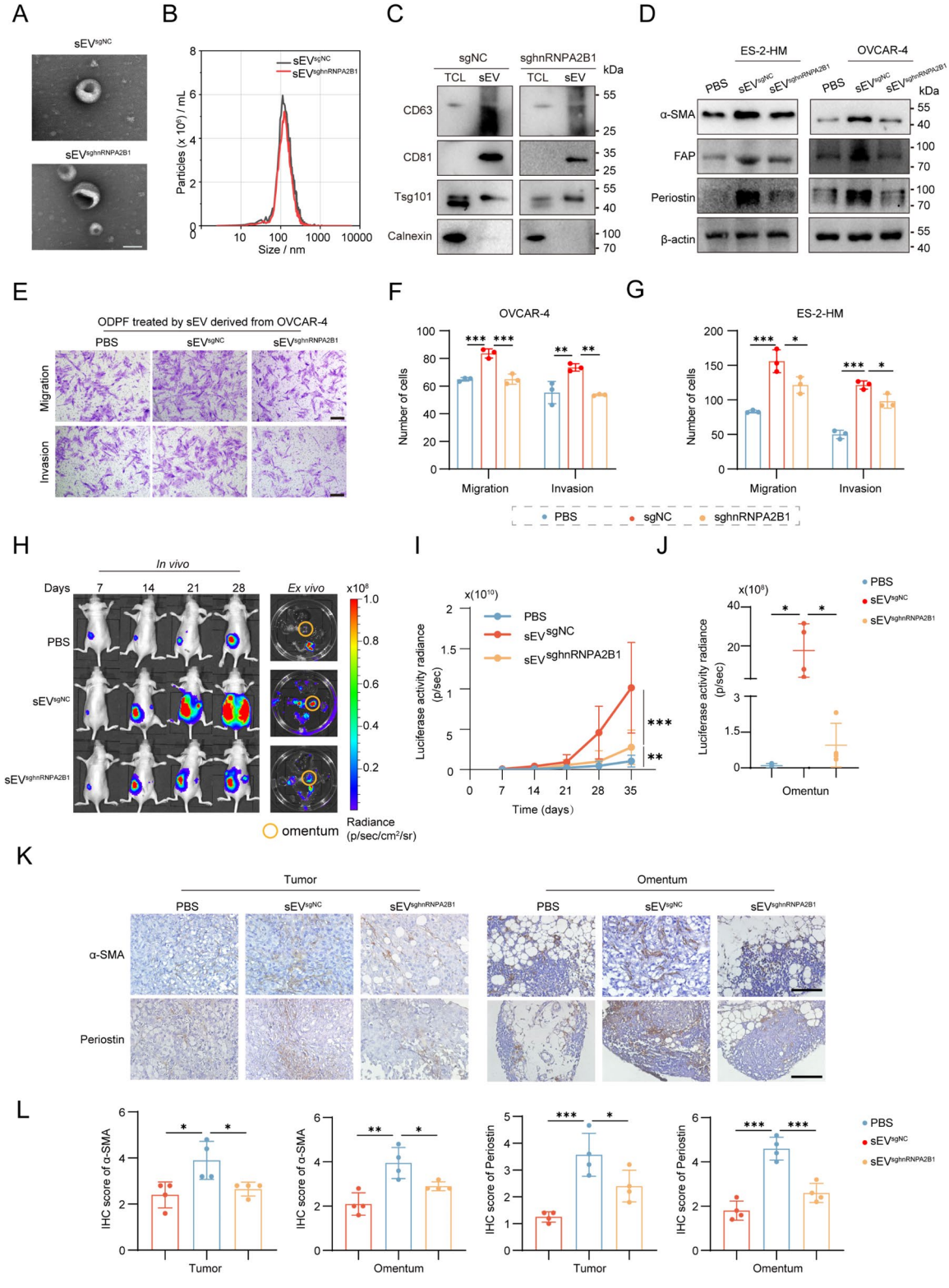

Fig. 4 (See legend on next page.)

(See figure on previous page.)

Fig. 4 Tumoral hnRNPA2B1 promotes omental metastasis and myofibroblast activation through small extracellular vesicles. (**A**) Representative transmission electron microscopy micrographs of small extracellular vesicles (sEVs) secreted by OVCAR-4 cells. Scale bar 100 nm. (**B**) Nanoparticle tracking analysis of sEVs secreted by OVCAR-4 cells. (**C**) Western blotting analysis of positive sEV markers (CD63, CD81, and Tsg101) and the negative marker Calnexin in total OvCa cells lysates (TCL) and the corresponding sEVs. (**D**) Western blot analysis of the α-SMA, FAP, and periostin levels in #1357 (left) ODPFs and #1368 (right) ODPFs treated with sEVs derived from OvCa cells. (**E**) Representative images of Transwell assays in #1370 ODPFs treated with PBS or the indicated sEVs derived from OVCAR-4 cells. Scale bar, 200 μm. (**F-G**) Quantification of Transwell assays for ODPFs treated with PBS or the indicated sEVs derived from OvCa cells. (**H**) Representative bioluminescence images of abdominal metastases in vivo (left) and abdominal organs isolated ex vivo after sacrifice (right) in the indicated groups. ($n = 4$ per group) (**I**) Bioluminescence signals at different observation points. (**J**) Scatter plot showing the bioluminescence signal of the omentum ex vivo. (**K-L**) Representative IHC images (**K**) and quantification (**L**) of α-SMA and periostin in tumor tissues and omental tissues from nude mice. Scale bar, 100 μm. *$P < 0.05$, **$P < 0.01$, ***$P < 0.001$

in paired omental tissues from OvCa patients (Fig. 3L-N, Table S5). These findings suggest that tumoral hnRNPA2B1 might be involved in omental myCAF activation in OvCa.

Tumoral hnRNPA2B1 facilitates omental metastasis and myofibroblast activation via small extracellular vesicles

The sEVs derived from OvCa tumor cells were purified from the conditioned medium using the differential ultracentrifugation method, as described previously [4]. Under a transmission electron microscope, the sEVs exhibited a saucer-shaped double-membrane structure with depression on one side (Fig. 4A). Nanoparticle tracking analysis was used to measure the size and number of vesicles. The results revealed that the peak concentration diameter of sEVs derived from OVCAR-4^{sgNC} cells was 136.1 nm, whereas for sEVs derived from OVCAR-4^{sghnRNPA2B1} cells, the peak concentration diameter was 137.4 nm. The proportion of sEV particles ranging from 50 to 200 nm was 80.99% for OVCAR-4 ^{sgNC} cells and 78.59% for OVCAR-4$^{sg-hnRNPA2B1}$ cells. These results confirmed the successful isolation of sEVs (Fig. 4B). Among the markers, sEVs expressed the positive markers CD63, CD81, and Tsg101 but not the negative marker calnexin (Fig. 4C). ODPFs were subsequently treated with PBS, sEV^{sgNC}, or sEV^{sghnRNPA2B1}. Western blotting revealed that the levels of the myCAF markers α-SMA, FAP, and periostin were significantly elevated in ODPFs treated with sEV^{sgNC} compared with those in ODPFs treated with the negative control (PBS) or sEV^{sghnRNPA2B1} (Fig. 4D, Fig. S4B-C). To investigate whether hnRNPA2B1 is present in the vesicle lumen of sEVs, dot blot assays were performed. The results revealed that CD63 was detectable on the surface of sEVs and was also present in the vesicle lumen, whereas hnRNPA2B1 was detected only under detergent-containing conditions (Fig. S5A). Functionally, Transwell assays demonstrated that sEV^{sgNC} notably enhanced the migration and invasion abilities of ODPFs compared with those of PBS or sEV^{sghnRNPA2B1} (Fig. 4E-G, Fig. S5B). Morphologically, ODPFs treated with sEV^{sgNC} had enlarged cell bodies and an extended spindle appearance compared with those treated with PBS or sEV^{sghnRNPA2B1} (Fig. S5C). Together, these data suggest that tumoral hnRNPA2B1 promotes myCAF activation via sEVs.

Subsequently, we explored whether the sEVs derived from tumoral hnRNPA2B1 promote OvCa omental metastasis *in vivo.* Spontaneous orthotopic tumor models in nude mice were established, and then the mice were intraperitoneally injected with PBS, sEV^{sgNC}, or sEV^{sghnRNPA2B1} (Fig. 4H). Compared with those in the sEV^{sghnRNPA2B1} or PBS group, the in vivo bioluminescence signals in the sEV^{sgNC} group exhibited a rapid increase (Fig. 4I). Ex vivo bioluminescence demonstrated that the bioluminescence signals in omental tissues were greater in the sEV^{sgNC} group than the sEV^{sghnRNPA2B1} or PBS groups (Fig. 4J). Additionally, we discovered that the levels of myCAF markers, as indicated by α-SMA and periostin, were greater in the sEV^{sgNC} group than in those from the sEV^{sghnRNPA2B1} or PBS groups (Fig. 4K-L). These results indicate that tumoral hnRNPA2B1 enhances the ability of sEVs to promote myCAF activation and OvCa omental metastasis.

Tumoral hnRNPA2B1 mediates miRNA sorting to small extracellular vesicles in a UAG sequence-dependent manner

Given the sorting function of hnRNPA2B1 in sEVs, the quantity and cargoes of sEV^{sgNC} and sEV^{sghnRNPA2B1} were analyzed. The particle counts, protein levels, and RNA levels of sEVs derived from equal numbers of cells were measured, and the results revealed no significant differences between sEV^{sgNC} and sEV^{sghnRNPA2B1} (Fig. 5A-C). Furthermore, sEV uptake assays were performed, and the results revealed that both sEV^{sgNC} and sEV^{sghnRNPA2B1} were taken up by ODPFs without notable differences (Fig. 5D). To screen the critical miRNAs sorted by hnRNPA2B1 in sEVs, high-throughput miRNA sequencing was performed on the sEV^{sgNC} and sEV^{sghnRNPA2B1} derived from OVCAR-4 cells. As shown in Fig. 5E, compared with those in sEV^{sgNC}, there were eleven significantly downregulated miRNAs and ten significantly upregulated miRNAs in sEV^{sghnRNPA2B1}. Among the eleven downregulated miRNAs, the six miRNAs (miR-21-5p, miR-224-5p, miR-92a-3p, miR-93-5p, miR-29a-3p, and miR-125a-5p) were enriched in the OVCAR-4 cells. To ascertain whether these miRNAs are transported from cells to sEVs, we compared the levels of miRNAs in both OvCa cells and their corresponding sEVs (Fig. 5F-G, Fig.

S6A). The results revealed significant increases in the sEV/cells ratios of miR-21-5p, miR-29a-3p, and miR-224-5p upon hnRNPA2B1 knockdown (Fig. 5H-I). To confirm that these miRNAs were contained within the sEVs, the sEVs were treated with RNase in the absence or presence of Triton X-100. The results revealed that the three highly enriched miRNAs were resistant to RNase in the absence of Triton X-100 (Fig. S6B). To explore the sorting ability of hnRNPA2B1 in vivo, we utilized sEVs derived from mice subcutaneous tumor tissues (sEV^{Tissue}) and the ascites of OvCa patients for validation. The sEV^{Tissue} levels of miR-21-5p, miR-29a-3p, and miR-224-5p in the sghnRNPA2B1 group were significantly lower than those in the sgNC group, whereas the total RNA levels of sEV^{Tissue} were not significantly different. (Fig. 5J-K). Furthermore, the lowest levels of miR-29a-3p and miR-224-5p in ODPFs treated with ascites-derived sEVs were coincident with the lowest level of hnRNPA2B1 in ascites-derived sEVs from the Patient #1094 compared with Patient #1121 and Patient #1296 (Fig. S6C-D, Table S5). Collectively, these results indicate that these miRNAs actively integrate into sEVs via a process regulated by hnRNPA2B1 in OvCa cells.

To examine the direct interaction between hnRNPA2B1 and these miRNAs, RIP assays and miRNA pull-down assays were performed. Compared with those in the IgG group, the groups treated with the hnRNPA2B1 antibody were significantly enriched (Fig. 5L). Further sequence analysis revealed that miR-21-5p, miR-29a-3p, and miR-224-5p all contain the UAG motif, a sequence that directly combines with hnRNPA2B1 [20] (Table S6). Wild-type and mutated miRNAs were labeled with biotin and then transfected into OvCa cells, followed by immunoprecipitation to detect hnRNPA2B1 protein levels. The results indicated that wild-type biotin-miRNAs interact with hnRNPA2B1, whereas the binding capacity was reduced when the UAG motif in the miRNAs was mutated (Fig. 5M). Moreover, dot-blot assays confirmed the presence of hnRNPA2B1 in the sEV^{sgNC} while revealing a reduced level of hnRNPA2B1 in the $sEV^{sghnRNPA2B1}$ derived from OvCa cells (Fig. S6E). These findings suggest that tumoral hnRNPA2B1 directly binds to the UAG motif in a sequence-dependent manner to assist in the sorting of miRNAs into sEVs.

Tumoral hnRNPA2B1 triggers myofibroblast activation through miRNAs enriched in small extracellular vesicles

To confirm whether sEV-miRNAs activate myCAFs, ODPFs were treated with sEV^{sgNC} or $sEV^{sghnRNPA2B1}$. Compared with those in ODPFs treated with sEV^{sgNC}, the mature miRNA levels were lower in the ODPFs treated with $sEV^{sghnRNPA2B1}$, while the levels of precursor miRNAs were not significantly different among the different groups (Fig. 6A-B). To elucidate the roles of miR-21-5p, miR-29a-3p, and miR-224-5p (miR-21/229/224) in myCAF activation, ODPFs were transfected with mimics of these miRNAs (Fig. S7A). Transwell assays and Western blotting were subsequently performed to explore the phenotypic modulation of myCAF activation, which was characterized by improved migration and invasion capacities as well as elevated levels of α-SMA, FAP, and periostin. The results showed that the upregulation of these miRNAs promoted myofibroblast activation (Fig. 6C-D, Fig. S7B, Fig. S9A). And up-regulation of miR-21-5p, miR-29a-3p, and miR-224-5p led to lower expression of PTEN (Fig. S7C). To determine whether miRNAs activation in myCAFs was induced by hnRNPA2B1-associated sEVs, ODPFs were treated with PBS, sEV^{sgNC}, $sEV^{sghnRNPA2B1}$, $sEV^{sghnRNPA2B1}$ combined with miR-21/229/224 mimics, or $sEV^{sghnRNPA2B1}$ combined with miRNA-NC mimics. We found that, compared with sEV^{sgNC}, $sEV^{sghnRNPA2B1}$ largely reduced ODPF migration and invasion, along with exhibiting low levels of α-SMA, FAP, and periostin. Furthermore, the upregulation of these miRNAs reversed the suppressive effect of $sEV^{sghnRNPA2B1}$ on myCAFs (Fig. 6E-F, Fig. S7D, Fig. S9B). These findings indicate that sEV-miRNAs activate myCAFs, which are regulated by hnRNPA2B1 in tumors.

To evaluate the pathways involved in myCAF activation, Kyoto Encyclopedia of Genes and Genomes (KEGG) analysis was performed on the target genes of the three miRNAs, and the results showed that the PI3K/AKT signaling pathway was significantly enriched (Fig. 6G). Gene set enrichment analysis (GSEA) of the GSE193875 dataset also revealed that the PI3K/AKT pathway was enriched in CAFs isolated from the OvCa patients with omental metastasis compared with that in CAFs without metastasis (Fig. 6H). Then, ODPFs were transfected with the miRNA mimics and exposed to MK2206 (an AKT inhibitor). Compared with the negative control, the miRNA mimics improved the α-SMA, FAP, and periostin levels, and increased the migratory and invasion capacities of ODPFs. Moreover, MK2206 largely inhibited PI3K/AKT pathway activation and partially reversed the myCAF activation induced by miRNA mimics (Fig. 6I-J, Fig. S8A, Fig. S9C). To assess the activation of the pathways induced by hnRNPA2B1-mediated sEVs, Western blotting assays was performed, and the results showed that sEV^{sgNC} activated the pathway in ODPFs compared with that in PBS or $sEV^{sghnRNPA2B1}$ (Fig. 6K, Fig. S9D). Then, ODPFs were exposed to PBS, sEV^{sgNC}, or sEV^{sgNC} combined with MK2206, and Western blotting assays were performed. The results showed that the PI3K/AKT inhibitor (MK2206) reversed the sEV^{sgNC}-induced activation of the PI3K/AKT pathway (Fig. S7B-E). In addition, the levels of the myCAF markers were significantly decreased in ODPFs treated with sEV^{sgNC} combined with MK2206 compared with those in ODPFs treated with

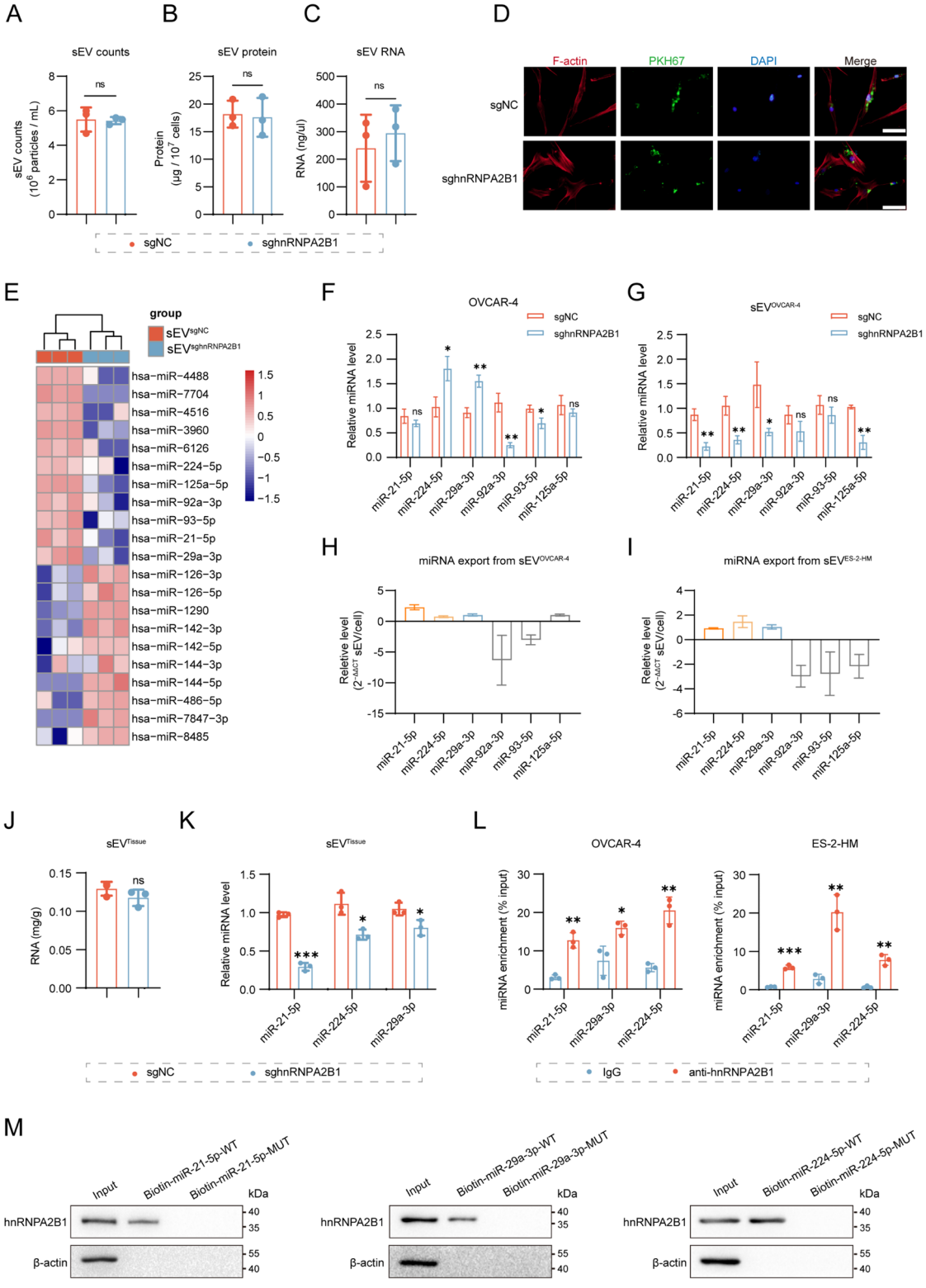

Fig. 5 (See legend on next page.)

(See figure on previous page.)

Fig. 5 Tumoral hnRNPA2B1 mediates miRNAs sorting to small extracellular vesicles in the UAG sequence-dependent manner. (**A-C**) The particle counts (**A**), the protein concentrations (**B**) and the RNA levels (**C**) in total small extracellular vesicles (sEVs) from equal amounts of cells were measured in OVCAR-4 cells. (**D**) Representative images of #1357 ODPFs uptake PKH67-labeled sEVs derived from OVCAR-4 cells. Red staining represents F-actin, green staining represents the PKH67-labeled sEVs, and blue staining represents DAPI. Scale bar, 100 μm (**E**) Hierarchical clustering analysis of miRNA expression profiles in sEVs derived from OVCAR-4 cells after hnRNPA2B1 downregulation. (**F-G**) Differential levels of six miRNAs in OVCAR-4 cells (**F**) and in sEVs (**G**) derived from OVCAR-4 cells with or without hnRNPA2B1 knockdown. (**H-I**) The sEV/cell ratio after hnRNPA2B1 knockdown of miRNAs between OvCa cells and sEVs in OVCAR-4 cells (**H**) or ES-2-HM cells (**I**). (**J**) The RNA quantitative analysis of total sEVs derived from subcutaneous tumor tissues. (**K**) qRT–PCR analysis of the level of the miRNAs in sEV derived from subcutaneous tumor tissues. (**L**) RIP assays showing that hnRNPA2B1 directly interacted with the miRNAs relative to IgG. (**M**) Western blot analysis of hnRNPA2B1 levels in samples derived from miRNA pulldowns performed in OVCAR-4 cells. *$P < 0.05$, **$P < 0.01$, ***$P < 0.001$; ns, not significant

sEV^{sgNC} (Fig. S7F-I). Functionally, Transwell assays demonstrated that MK2206 notably rescued the enhanced the migration and invasion abilities of ODPFs induced by sEV^{sgNC} (Fig. S7J-M). These findings strongly support the role of the PI3K/AKT pathway in tumoral hnRNPA2B1-mediated myCAF activation. To explore whether sEV-miRNAs affected by hnRNPA2B1 trigger this pathway, ODPFs were treated with PBS, sEV^{sgNC}, $sEV^{sghnRNPA2B1}$, $sEV^{sghnRNPA2B1}$ combined with miR-21/229/224 mimics, or $sEV^{sghnRNPA2B1}$ combined with miR-NC mimics. We found that the upregulation of miRNAs counteracted the inhibition of the PI3K/AKT pathway induced by $sEV^{sghnRNPA2B1}$ (Fig. 6L, Fig. S9E). These results indicate that sEVs trigger the PI3K/AKT pathway to activate myCAFs via a process mediated by hnRNPA2B1 in OvCa cells.

Tumoral hnRNPA2B1 activates myofibroblasts to promote tumor metastasis

To determine the impact of sEV-activated myCAFs on OvCa cells, we treated OvCa cells with conditioned medium (CM) from ODPFs which treated with PBS, sEV^{sgNC}, or $sEV^{sghnRNPA2B1}$. Transwell assays showed that sEV^{sgNC} group significantly promoted the migration and invasion of OvCa cells compared with PBS, and $sEV^{sghnRNPA2B1}$ inhibited these abilities in comparison with sEV^{sgNC} (Fig. 7A-C, Fig. S8N). To further determine the role of myCAFs activated by sEV-miRNAs in OvCa cells, ODPFs were pre-cocultured with PBS, sEV^{sgNC}, or $sEV^{sghnRNPA2B1}$, and ODPFs in the $sEV^{sghnRNPA2B1}$ group were transfected with miRNA mimics, followed by incubation with MK2206. The CM collected from the ODPFs of various groups was utilized for treating OvCa cells. Transwell assays showed that miRNA mimics partially reversed the decreased invasion and migration capabilities of OvCa cells induced by $sEV^{sghnRNPA2B1}$, and MK2206 attenuated the enhanced migration and invasion abilities of OvCa cells improved by the miRNA mimics (Fig. 7D-E). To validate the metastasis-promoting role of myCAFs activated by tumoral hnRNPA2B1 in vivo, nude mice were intraperitoneally injected with sgNC or sghnRNPA2B1 cells, and mice injected with sghnRNPA2B1 cells were treated with agomiR-21/29/224 and MK2206 (Fig. 7F). In vivo bioluminescence imaging indicated that the abdominal signals in the sghnRNPA2B1 group were significantly lower than those in the sgNC group. Moreover, agomiR-21/29/224 reversed the negative effects of sghnRNPA2B1, and MK2206 notably suppressed these effects (Fig. 7G). Moreover, the trend of the bioluminescence signals in vivo was mirrored by the bioluminescence intensity of the abdominal organ ex vivo (Fig. 7H). Similarly, our findings revealed that sghnRNPA2B1 reduced the levels of α-SMA and periostin in the omental tissues of mice compared with sgNC. Moreover, agomiR-21/29/224 effectively restored the decreased levels of α-SMA and periostin in sghnRNPA2B1 cells. Additionally, treatment with MK2206 mitigated the increase in the levels of α-SMA and periostin that were attenuated by agomiR-21/29/224 (Fig. 7I-K). In summary, these results collectively demonstrated that tumoral hnRNPA2B1 activates myCAF via the PI3K/AKT pathway to promote tumor metastasis.

Discussion

Multiple mechanisms regulate intercellular communication in TME, where sEV-miRNAs play crucial roles [21]. However, the specific mechanisms underlying the loading of miRNAs into sEVs are still unknown. In this study, we identified a novel function of the hnRNPA2B1 protein in the selective packaging of metastasis-promoting miRNAs into sEVs, and provided new insight into how RBPs promote the distant metastasis of OvCa through the sEV sorting mechanism.

hnRNPA2B1, an RBP belonging to the hnRNP family that is highly conserved across various species, is significantly overexpressed in multiple types of tumors [7, 17]. In this study, we discovered that hnRNPA2B1 is upregulated in OvCa and plays a role in promoting tumor metastasis, which is in line with previous investigations of colon cancer [22] and pancreatic cancer [23]. As an RBP, hnRNPA2B1 is extensively involved in the regulation of RNA molecules to promote tumor progression [24]. Our previous study has demonstrated the role of hnRNPA2B1 in maintaining CDK19 mRNA stability in an m^6A-dependent manner in OvCa [18]. Recent studies have implicated hnRNPA2B1 in the trafficking and maturation of miRNAs [25–27]. To date, little evidence from studies has shown the involvement of hnRNPA2B1 in the

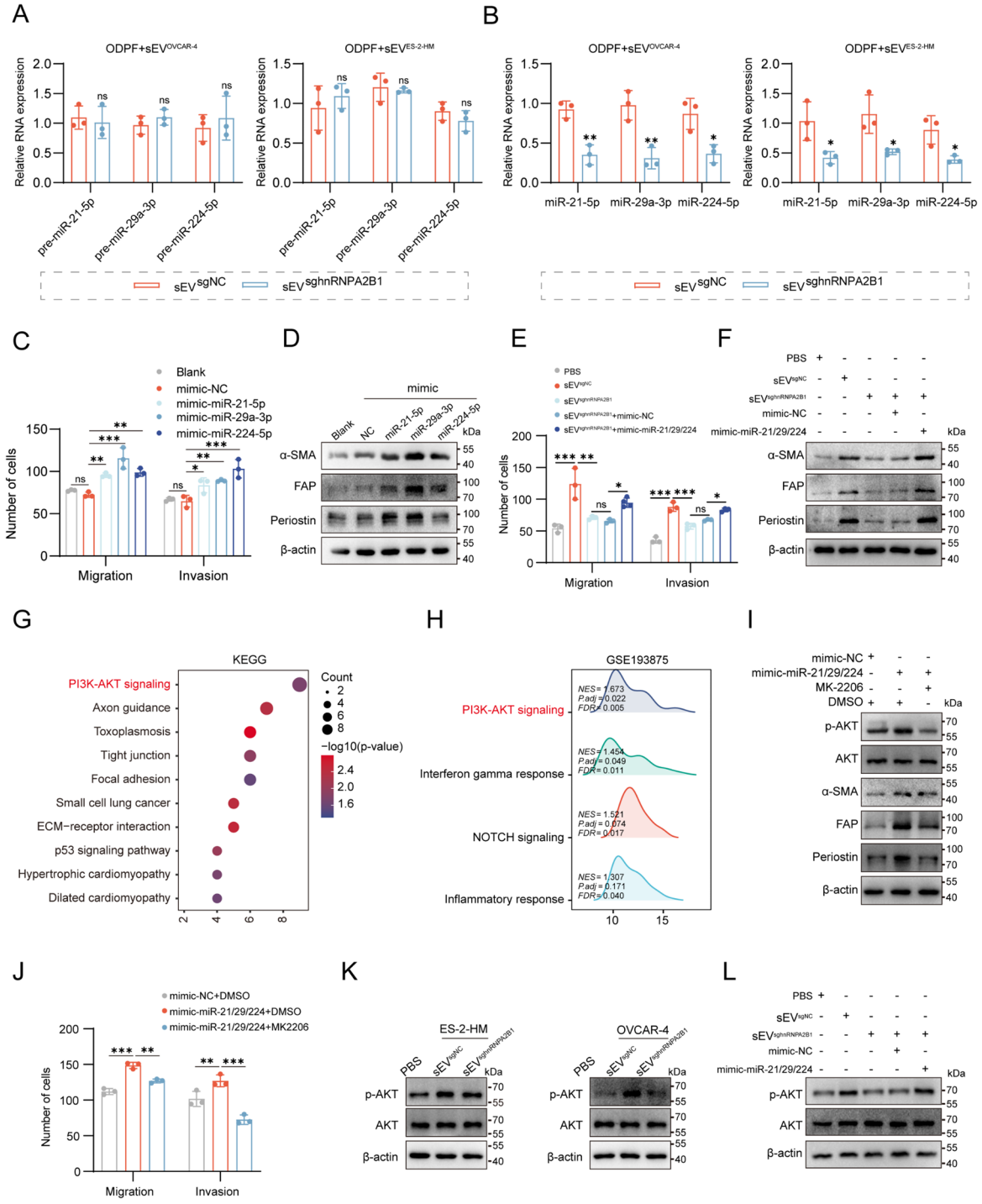

Fig. 6 Tumoral hnRNPA2B1 induces myofibroblast activation through miRNAs enriched in small extracellular vesicles. (A-B) qRT-PCR analysis of the levels of pre-miRNAs and mature miRNAs in ODPFs treated with sEV^{sgNC} or $sEV^{sghnRNPA2B1}$. (**C**) Quantification of Transwell assays in ODPFs after the overexpression of three miRNAs. (**D**) Western blot analysis of the α-SMA, FAP, and periostin levels in #1371 ODPFs after the overexpression of the three miRNAs. (**E**) Quantification of ODPFs Transwell assays in the indicated groups. (**F**) Western blot analysis of α-SMA, FAP, and periostin levels in #1488 ODPFs in the above groups. (**G**) KEGG pathway enrichment analysis of genes targeted by miR-21-5p, miR-29a-3p, and miR-224-5p. (**H**) GSEA of CAFs with or without omental metastases in the GSE193875. (**I**) Western blot analysis of the α-SMA, FAP, periostin, AKT, and phosphorylated AKT (p-AKT) level in #1505 ODPFs in the specified group. (**J**) Quantification of ODPFs Transwell assays in the mentioned group. (**K**) Western blot analysis of AKT and p-AKT levels in #1404 ODPFs (left) or #1426 ODPFs (right) cocultured with sEV^{sgNC} or $sEV^{sghnRNPA2B1}$ derived from ES-2-HM (left) or OVCAR-4 cells (right). (**L**) Western blot analysis of AKT and p-AKT levels in #1395 ODPFs in the indicated groups. $^{*}P < 0.05$, $^{**}P < 0.01$, $^{***}P < 0.001$; ns, not significant

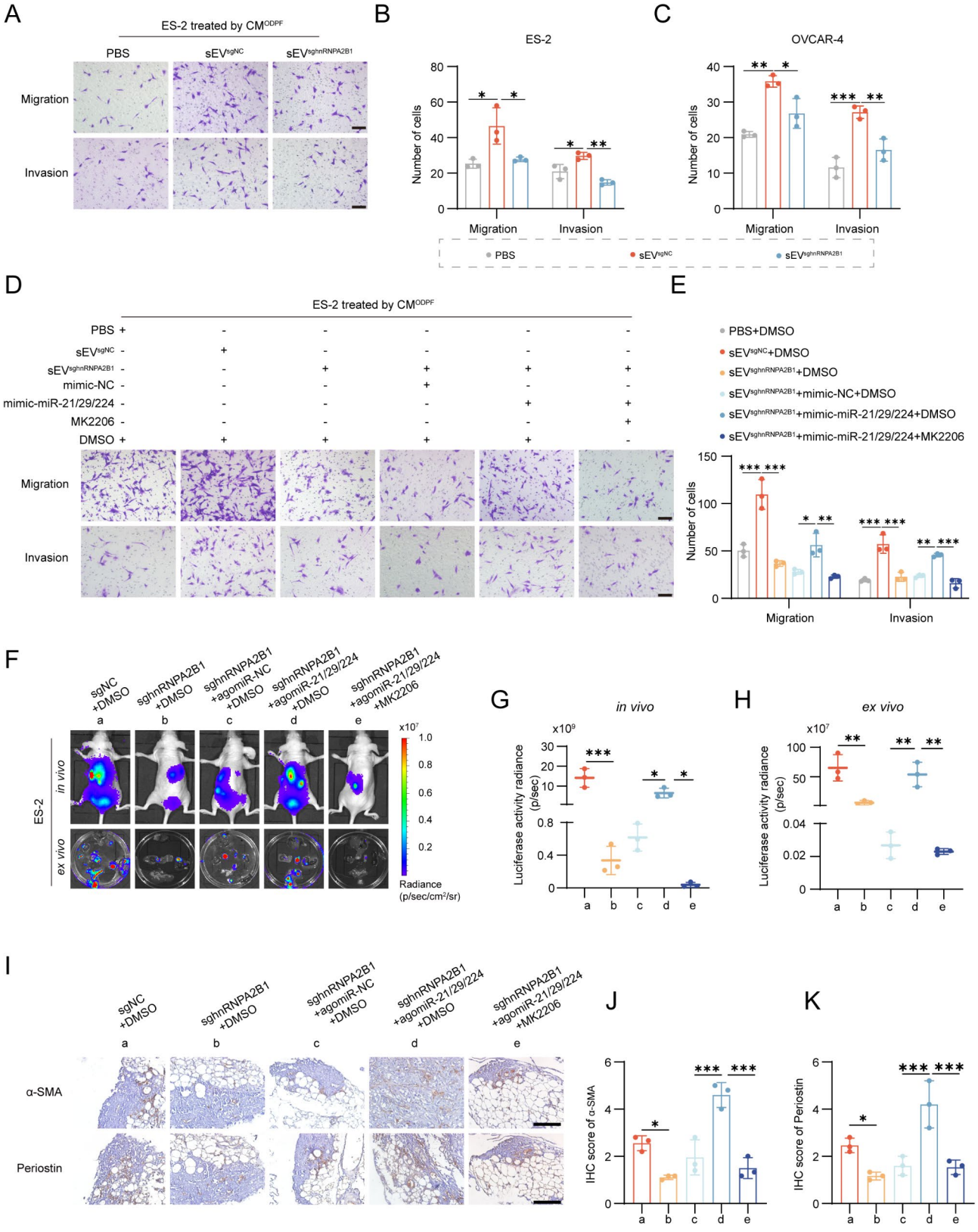

Fig. 7 (See legend on next page.)

(See figure on previous page.)

Fig. 7 Tumoral hnRNPA2B1 activates myofibroblasts to promote tumor metastasis. (**A**) Representative images of Transwell assays of ES-2 cells exposed to conditioned medium (CM) from ODPFs precocultured with PBS, sEV^{sgNC}, or $sEV^{sghnRNPA2B1}$ derived from OvCa cells. Scale bar, 100 μm. (**B-C**) Histogram analysis of Transwell assays of ODPFs in ES-2 or OVCAR-4 cells in the mentioned groups. (**D-E**) Representative images and quantification of Transwell assays of ES-2 cells exposed to the CM from ODPFs in indicated groups. Scale bar 100 μm. (**F**) Representative bioluminescence images of abdominal metastases in vivo (above) and abdominal organs isolated after sacrifice ex vivo (below) in the indicated groups ($n = 3$ per group). (**G-H**) Scatter plot showing the bioluminescence signal in vivo (**G**) and the bioluminescence signal of all abdominal organs ex vivo (**H**). (**I-K**) Representative IHC images (**I**) and quantification of α-SMA (**J**) and periostin (**K**) in omental tissues from nude mice. Scale bar, 100 μm. $^{*}P < 0.05$, $^{**}P < 0.01$, $^{***}P < 0.001$

sorting process in OvCa. This study highlights the crucial role of hnRNPA2B1 in the loading of cargoes into sEVs. Typically, when an RNA is sorted into sEVs, its expression within the cells usually decreases because a portion of the RNA molecule is transported to the sEVs. However, in our investigation, an intriguing pattern emerged following the knockout of hnRNPA2B1, not only did the sorting of miR-21-5p into sEVs diminish, but the intracellular level of miR-21-5p also slightly decreased. This observation highlights the intricate and multifaceted biological functions of hnRNPA2B1 in vivo. hnRNPA2B1 may promote the maturation of pri-miRNAs in an m^6A-dependent manner [28]. Consequently, the knockdown of hnRNPA2B1 not only impacts the maturation of intracellular miRNA but also potentially disrupts the sorting process into sEVs, ultimately resulting in a slight decrease in miRNA levels within the cell.

Certain conserved RNA motifs typically function as recognition sites for protein structural elements, enabling the release of the sEVs. The GGAG motif is the first reported miRNA sequence implicated in sEV sorting and has subsequently been confirmed across various diseases [26, 29, 30]. Recent protein structure analysis revealed that hnRNPA2B1 specifically recognizes the AGG and UAG motifs through its two RNA recognition domains [20]. Here, RNA pulldown and RIP assays revealed that hnRNPA2B1 binds to miR-21-5p, miR-29a-3p, and miR-224-5p in a UAG sequence-dependent manner. Conversely, research has reported that hnRNPA2B1 inhibits the sorting of sEVs from miR-503 [31]. These findings suggest that hnRNPA2B1 may be involved in different mechanisms of sEV sorting, resulting in diverse sorting outcomes. Communication between tumor cells and stromal cells is crucial for promoting the metastatic TME [32]. Recent studies have revealed the functional heterogeneity of CAFs, demonstrating that they belong to diverse subgroups [33]. Among these subgroups, myCAFs promote tumor metastasis through extracellular matrix deposition and remodeling. In our investigation, we identified miR-21-5p, miR-29a-3p, and miR-224-5p enclosed in tumor-derived sEVs as important factors in the activation of omental myCAFs. Overexpression of miR-21-5p has been shown to significantly enhance fibroblast activity, including proliferation, migration, and fibrogenesis [34]. Similarly, miR-224 has been found to be related to fibrosis in chronic hepatitis patients [35]. Notably, miR-29a-3p overexpression inhibits fibroblast activation [36]. These results can be attributed to the heterogeneity in the functions of miRNAs across various diseases, particularly tumoral conditions [37–40]. Further investigations are needed to explore this phenomenon.

Conclusions

This study provides novel insights into the role of hnRNPA2B1 in mediating the trafficking of miRNAs into sEVs in OvCa, which activates omental myCAFs to promote OvCa metastasis. This discovery offers novel perspectives on the intricate mechanisms of the selective sorting of RBP-miRNA complexes within sEVs, which may illuminate new therapeutic strategies.

Abbreviations

sEVs	Small extracellular vesicles
OvCa	Ovarian carcinoma
TME	Tumor microenvironment
CAF	Cancer-associated fibroblast
myCAFs	Myofibroblasts
RBPs	RNA-binding proteins
hnRNPs	Heterogeneous nuclear ribonucleoprotein
ODPFs	Omental-derived primary fibroblasts
RIP	RNA immunoprecipitation
CM	Conditioned medium

Supplementary Information

The online version contains supplementary material available at https://doi.org/10.1186/s12951-025-03342-w.

Supplementary Material 1

Supplementary Material 2

Acknowledgements

The graphical abstract is created with BioRender.com.

Author contributions

Q.W. and P.L. conducted most of the experimental work and wrote the manuscript. J.C. conceived the project. Z.W. and L.Y. supervised the project. X.L., L.H., and F.Y. performed the animal experiments. G.L., W.L. and J.Z. collected the clinical samples. L.G., R.G., X.Y., and L.X. analyzed the clinical data. All authors read and approved.

Funding

This work was supported by the National Natural Science Foundation of China (No.82473095, No.81974413, and No.82303514), the Natural Science Foundation of Hubei Province of China (No.2022CFB107 and No.2022CFB147), and the Science Technology Foundation of Hubei Province of China (No.2023AFB1070).

Data availability

No datasets were generated or analysed during the current study.

Declarations

Ethics approval and consent to participate
This study was performed in accordance with the Declaration of Helsinki. All clinical specimens and information involved in this study provided informed consent before collection and were approved by The Ethics Committee of Tongji Medical College, Huazhong University of Science and Technology (IORG No: IORG0003571). All animal study procedures were approved by the Institutional Animal Care and Use Committee of Wuhan Youdu Biological Technology (WHYDSW No.20221219).

Consent for publication
Not applicable.

Competing interests
The authors declare no competing interests.

Author details
[1]Department of Obstetrics and Gynecology, Union Hospital, Tongji Medical College, Huazhong University of Science and Technology, Wuhan 430022, China

Received: 26 August 2024 / Accepted: 20 March 2025
Published online: 04 April 2025

References

1. Siegel RL, Kratzer TB, Giaquinto AN, Sung H, Jemal A. Cancer statistics, 2025. CA Cancer J Clin. 2025;75(1):10–45.
2. Wang SE. Extracellular vesicles in cancer therapy. Semin Cancer Biol. 2022;86(Pt 2):296–309.
3. Caligiuri G, Tuveson DA. Activated fibroblasts in cancer: perspectives and challenges. Cancer Cell. 2023;41(3):434–49.
4. Li G, Yi X, Du S, Gong L, Wu Q, Cai J, et al. Tumour-derived Exosomal piR-25783 promotes omental metastasis of ovarian carcinoma by inducing the fibroblast to myofibroblast transition. Oncogene. 2023;42(6):421–33.
5. Zhu G, Wang Y, Wang Y, Huang H, Li B, Chen P, et al. Myofibroblasts derived type V collagen promoting tissue mechanical stress and facilitating metastasis and therapy resistance of lung adenocarcinoma cells. Cell Death Dis. 2024;15(7):493.
6. Feng W, Dean DC, Hornicek FJ, Shi H, Duan Z. Exosomes promote pre-metastatic niche formation in ovarian cancer. Mol Cancer. 2019;18(1):124.
7. Guo Q, Fan Y, Wang Q, Li B, Qiu W, Qi Y, et al. Glioblastoma upregulates sumoylation of HnRNP A2/B1 to eliminate the tumor suppressor miR-204-3p, accelerating angiogenesis under hypoxia. Cell Death Dis. 2023;14(2):147.
8. Kosaka N, Iguchi H, Hagiwara K, Yoshioka Y, Takeshita F, Ochiya T. Neutral Sphingomyelinase 2 (nSMase2)-dependent Exosomal transfer of angiogenic MicroRNAs regulate cancer cell metastasis. J Biol Chem. 2013;288(15):10849–59.
9. Koppers-Lalic D, Hackenberg M, Bijnsdorp IV, van Eijndhoven MAJ, Sadek P, Sie D, et al. Nontemplated nucleotide additions distinguish the small RNA composition in cells from exosomes. Cell Rep. 2014;8(6):1649–58.
10. Guduric-Fuchs J, O'Connor A, Camp B, O'Neill CL, Medina RJ, Simpson DA. Selective extracellular vesicle-mediated export of an overlapping set of MicroRNAs from multiple cell types. BMC Genomics. 2012;13:357.
11. Fabbiano F, Corsi J, Gurrieri E, Trevisan C, Notarangelo M, D'Agostino VG. RNA packaging into extracellular vesicles: an orchestra of RNA-binding proteins? J Extracell Vesicles. 2020;10(2):e12043.
12. Zietzer A, Hosen MR, Wang H, Goody PR, Sylvester M, Latz E, et al. The RNA-binding protein HnRNPU regulates the sorting of microRNA-30c-5p into large extracellular vesicles. J Extracell Vesicles. 2020;9(1):1786967.
13. Xu YF, Xu X, Gin A, Nshimiyimana JD, Mooers BHM, Caputi M, et al. SRSF1 regulates exosome MicroRNA enrichment in human cancer cells. Cell Commun Signal. 2020;18(1):130.
14. Shurtleff MJ, Temoche-Diaz MM, Karfilis KV, Ri S, Schekman R. Y-box protein 1 is required to sort MicroRNAs into exosomes in cells and in a cell-free reaction. Elife 2016; 5.
15. Qin H, Ni H, Liu Y, Yuan Y, Xi T, Li X, et al. RNA-binding proteins in tumor progression. J Hematol Oncol. 2020;13(1):90.
16. Bitaraf A, Razmara E, Bakhshinejad B, Yousefi H, Vatanmakanian M, Garshasbi M, et al. The oncogenic and tumor suppressive roles of RNA-binding proteins in human cancers. J Cell Physiol. 2021;236(9):6200–24.
17. Liu Y, Shi SL. The roles of HnRNP A2/B1 in RNA biology and disease. Wiley Interdiscip Rev RNA. 2021;12(2):e1612.
18. Wu Q, Li G, Gong L, Cai J, Chen L, Xu X et al. Identification of miR-30c-5p as a tumor suppressor by targeting the m(6) A reader HNRNPA2B1 in ovarian cancer. Cancer Med 2022.
19. Ying F, Guo J, Gao X, Huang L, Gao L, Cai J, et al. Establishment of highly metastatic ovarian cancer model with omental tropism via in vivo selection. iScience. 2023;26(5):106719.
20. Wu B, Su S, Patil DP, Liu H, Gan J, Jaffrey SR, et al. Molecular basis for the specific and multivariant recognitions of RNA substrates by human HnRNP A2/B1. Nat Commun. 2018;9(1):420.
21. de Visser KE, Joyce JA. The evolving tumor microenvironment: from cancer initiation to metastatic outgrowth. Cancer Cell. 2023;41(3):374–403.
22. Liu H, Li D, Sun L, Qin H, Fan A, Meng L, et al. Interaction of LncRNA MIR100HG with hnRNPA2B1 facilitates m(6)A-dependent stabilization of TCF7L2 mRNA and colorectal cancer progression. Mol Cancer. 2022;21(1):74.
23. Meng LD, Shi GD, Ge WL, Huang XM, Chen Q, Yuan H, et al. Linc01232 promotes the metastasis of pancreatic cancer by suppressing the ubiquitin-mediated degradation of HNRNPA2B1 and activating the A-Raf-induced MAPK/ERK signaling pathway. Cancer Lett. 2020;494:107–20.
24. Yang Y, Wei Q, Tang Y, Yuanyuan W, Luo Q, Zhao H, et al. Loss of hnRNPA2B1 inhibits malignant capability and promotes apoptosis via down-regulating Lin28B expression in ovarian cancer. Cancer Lett. 2020;475:43–52.
25. Qi F, Shen W, Wei X, Cheng Y, Xu F, Zheng Y, et al. CSNK1D-mediated phosphorylation of HNRNPA2B1 induces miR-25-3p/miR-93-5p maturation to promote prostate cancer cell proliferation and migration through m(6) A-dependent manner. Cell Mol Life Sci. 2023;80(6):156.
26. Villarroya-Beltri C, Gutierrez-Vazquez C, Sanchez-Cabo F, Perez-Hernandez D, Vazquez J, Martin-Cofreces N, et al. Sumoylated hnRNPA2B1 controls the sorting of MiRNAs into exosomes through binding to specific motifs. Nat Commun. 2013;4:2980.
27. Zhou X, Hong Y, Liu Y, Wang L, Liu X, Li Y, et al. Intervening in hnRNPA2B1-mediated Exosomal transfer of tumor-suppressive miR-184-3p for tumor microenvironment regulation and cancer therapy. J Nanobiotechnol. 2023;21(1):422.
28. Alarcon CR, Goodarzi H, Lee H, Liu X, Tavazoie S, Tavazoie SF. HNRNPA2B1 is a mediator of m(6)A-Dependent nuclear RNA processing events. Cell. 2015;162(6):1299–308.
29. Si Y, Liu F, Wang D, Fang C, Tang X, Guo B, et al. Exosomal transfer of miR-185 is controlled by hnRNPA2B1 and impairs Re-endothelialization after vascular injury. Front Cell Dev Biol. 2021;9:619444.
30. Li C, Qin F, Wang W, Ni Y, Gao M, Guo M et al. hnRNPA2B1-Mediated extracellular vesicles sorting of miR-122-5p potentially promotes lung cancer progression. Int J Mol Sci 2021; 22(23).
31. Perez-Boza J, Boeckx A, Lion M, Dequiedt F, Struman I. hnRNPA2B1 inhibits the Exosomal export of miR-503 in endothelial cells. Cell Mol Life Sci. 2020;77(21):4413–28.
32. Beltraminelli T, Perez CR, De Palma M. Disentangling the complexity of tumor-derived extracellular vesicles. Cell Rep. 2021;35(1):108960.
33. Yu S, Yang R, Xu T, Li X, Wu S, Zhang J. Cancer-associated fibroblasts-derived FMO2 as a biomarker of macrophage infiltration and prognosis in epithelial ovarian cancer. Gynecol Oncol 2022.
34. Wu XD, Kang L, Tian J, Wu Y, Huang Y, Liu J, et al. Exosomes derived from magnetically actuated bone mesenchymal stem cells promote tendon-bone healing through the miR-21-5p/SMAD7 pathway. Mater Today Bio. 2022;15:100319.
35. Appourchaux K, Dokmak S, Resche-Rigon M, Treton X, Lapalus M, Gattolliat CH, et al. MicroRNA-based diagnostic tools for advanced fibrosis and cirrhosis in patients with chronic hepatitis B and C. Sci Rep. 2016;6:34935.
36. Luo Y, Dong HY, Zhang B, Feng Z, Liu Y, Gao YQ, et al. miR-29a-3p attenuates hypoxic pulmonary hypertension by inhibiting pulmonary adventitial fibroblast activation. Hypertension. 2015;65(2):414–20.
37. Cao J, Zhang Y, Mu J, Yang D, Gu X, Zhang J. Exosomal miR-21-5p contributes to ovarian cancer progression by regulating CDK6. Hum Cell. 2021;34(4):1185–96.
38. Lu L, Ling W, Ruan Z. TAM-derived extracellular vesicles containing microRNA-29a-3p explain the deterioration of ovarian cancer. Mol Ther Nucleic Acids. 2021;25:468–82.

39. Krasniqi E, Sacconi A, Marinelli D, Pizzuti L, Mazzotta M, Sergi D, et al. MicroRNA-based signatures impacting clinical course and biology of ovarian cancer: a mirnomics study. Biomark Res. 2021;9(1):57.
40. Lee KS, Lee J, Kim HK, Yeom SH, Woo CH, Jung YJ, et al. Extracellular vesicles from adipose tissue-derived stem cells alleviate osteoporosis through osteoprotegerin and miR-21-5p. J Extracell Vesicles. 2021;10(12):e12152.

Publisher's note